Journal of Materials Science & Technology 35 (2019) 2734–2741

Contents lists available at ScienceDirect

Journal of Materials Science & Technology

journal homepage: www.jmst.org

Research Article

Fabrication, characterization and optimization of high conductivity and high quality nanocrystalline molybdenum thin films

Anil K. Battu[a,b], Nanthakishore Makeswaran[a], C.V. Ramana[a,*]

[a] Center for Advanced Materials Research (CMR), University of Texas at El Paso, El Paso, TX 79968, USA
[b] Environmental Molecular Sciences Laboratory (EMSL), Pacific Northwest National Laboratory (PNNL), Richland, WA 99352, USA

ARTICLE INFO

Article history:
Received 24 January 2019
Received in revised form 9 April 2019
Accepted 30 April 2019
Available online 22 May 2019

Keywords:
Molybdenum
Thin films
Microstructure
Electrical characteristics
Optical properties
Solar cells

ABSTRACT

The present study investigated the influence of substrate temperature (T_s) and working pressure (P_{Ar}) on tailoring the properties of nanocrystalline (nc) molybdenum (Mo) films fabricated by radio-frequency magnetron sputtering. The structural, morphological, electrical and optical properties of nc-Mo films were evaluated in detail. The Mo films exhibited (110) orientation with average crystallite size varying from 9 to 22 (±1) nm on increasing T_s. Corroborating with structural data, the electrical resistivity decreased from 55 μΩ cm to 10 μΩ cm, which is the lowest among all the Mo films. For Mo films deposited under variable P_{Ar}, the (110) peak intensity decrement coupled with peak broadening on increasing P_{Ar}. Lower deposition pressure yielded densely packed thin films with superior structural properties along with low resistivity of ~15 μΩ cm. Optimum conditions to produce high quality Mo films with excellent structural, morphological, electrical and optical characteristics for utilization in solar cells as back contact layers were identified.

1. Introduction

Manipulating the structure and properties of solid-state materials at nanoscale dimensions has emerged as an optimal tool to unlock the full potential of materials in renewable energy technologies, particularly those aimed at utilizing solar energy. Controlling over structure/property/processing correlations in nanomaterials is a critical aspect of cutting-edge research in the application of material science and nanotechnology for energy related technologies [1–7]. The physical, structural, chemical and electronic properties of these nanomaterials are highly sensitive to the processing conditions they are manufactured in and as a result these microstructures can often be tuned to meet the requirements of a given energy related technological application [8–10]. Both physical and chemical synthetic methods can be used to alter or control these microstructures.

Solar cell technology, a means of harvesting one of the most promising available renewable energy resources, can convert sunlight directly into electric power without any greenhouse gases or pollutant emissions into the environment [11]. While solar cell devices are a stack with a multi-layered configurations, the back contact layers are quite important in thin film solar cell technology, as they can offer an economic and expedited manufacturing process compared to traditional fabrication methods used for silicon wafer-based solar cells [1,12]. For instance, Cadmium Telluride (CdTe), Copper Indium Selenide (CIS), Copper Indium Gallium Selenide (CIGS) and Copper Zinc Tin Sulfide (CZTS) solar cells are popular and currently preferred methodologies for efficient conversion and utilization of solar energy [1,12–19]. High stability of CdTe solar cells is considered as an important factor for space applications [11]. Recently, tin (II) sulfide (SnS) based solar cell technology is also emerging as an alternative [20]. The theoretical conversion efficiency limit of SnS solar cells is higher than 20%. Thus, SnS is also promising material for photovoltaic applications; it exhibits a bandgap of 1.1–1.5 eV and excellent optical absorption value $\alpha > 10^4\ cm^{-1}$ [20]. There is an enormous interest in the development of CIS and CIGS solar cells on flexible or organic substrates due to their low cost, light weight, high specific power density and excellent radiation hardness [3,12,14–18]. However, such rapid development of CIS/CIGS solar cells and further progress in the field depend on the efficient design and development of high-quality component layers, such as back contact metallic films, which can offer improved physical, chemical and electronic properties while serving under the elevated processing conditions [12,21]. While there are many options available for suitable materials, due to a wide variety of scientific reasons and its

* Corresponding author.
E-mail address: rvchintalapalle@utep.edu (C.V. Ramana).

https://doi.org/10.1016/j.jmst.2019.05.023
1005-0302/

material properties, molybdenum (Mo) has emerged as the predominant choice for the back-contact layer application in CIGS/CIS solar cells [14,17,18,22–24].

Molybdenum is a refractory metal; fascinating properties of Mo have been exploited in a wide variety of industrial applications [14,15,18,21,25–30]. The high melting point (2160 °C), low density (ρ_{th} = 10.2 g/cm^3) and excellent strength-to-density ratio at high temperature make Mo attractive, even compared to other refractory metals, for many applications in aerospace, defense, and energy sectors. In the context of thin film solar cells, sputter-deposited Mo films were widely used as back contact layers in CIS and CIGS solar cells [15,31–35]. The back contact layer forms the substrate upon which the light absorbent layer fabrication proceeds in the solar cell design [14,15,18]. Mo has been identified as an ideal choice for the back contact in CIS and CIGS solar cells not only due to its excellent electrical properties but also for its inertness and mechanical durability during the absorber film growth [14,15,18,36]. The challenge now revolves around maintaining a metallic state, i.e. without oxidation, and retaining the structural quality and desirable electrical properties of Mo at the high processing temperatures common to thin film solar cell technology [5,15,37–39].

For thin film Mo, most of the existing studies employed direct current (DC) magnetron sputtering. It has been noted that the resistivity and adhesion of Mo films are strongly dependent on the working gas pressure [40,41]. Higher sputtering gas pressures tend to yield highly adhesive, and highly resistive Mo films. Alternatively, lower pressures result in low resistivity but poor mechanical properties and adhesion [14,15,18,40,41]. A correlation is also observed between the sputter gas pressures (P_{Ar}) and cumulative stress within deposited films [21]. Generally, the films deposited with low P_{Ar} are found to be under compressive stress, while those deposited with high pressures are found to be under tensile stress [21]. Recently, it has been demonstrated that the radio-frequency (RF) magnetron sputtering represents an alternative approach to deposit high-quality Mo films for electronic and optoelectronic applications [3,16,41,42]. Jubault et al. demonstrated that good adhesion of Mo layers could be obtained within a much wider range of sputtering pressures, with electrical properties being less sensitive to the sputtering parameters [3]. Additionally Zoppi et al. reported that Mo films with a low resistivity (21.3 μΩ cm) can be obtained for deposition at room temperature through the manipulation of the RF process parameters [18]. It should be noted that these Mo films were amorphous and post-deposition annealing performed at 530 °C in Ar and H_2/N_2 in order to further improve the film crystal quality resulted in an increased resistivity of Mo film due to possible surface oxidation [18]. This annealing also deteriorated the films adhesion properties [18]. Wang et al. also reported a low resistivity of 22.8 μΩ cm for Mo films by RF sputtering by using a slightly higher deposition temperature (200 °C) [41]. However, further increasing deposition temperatures showed a degradation in the overall properties [41]. Most recently, Dai et al. demonstrated the superior characteristics of Mo films deposited by RF sputtering [16]. In their work, Mo films were deposited at an elevated deposition temperature (400 °C) with varying sputtering power and sputtering gas pressures. These authors reported that lower pressure and higher power of RF sputtering can result in Mo films with lower resistivity due to increased kinetic energy of sputtered particles, which in turn improved the crystalline nature and compactness of the films [16]. However, while desirable electrical properties can be obtained, adhesion properties of the Mo films were very poor [16]. Thus, significant attention is being directed to the structure and electronic property control of Mo films while maintaining the good mechanical properties of the layers. Also, structural quality and property degradation of Mo films deposited at elevated temperatures and/or during post-deposition annealing are of much concern, particularly for their utilization in polycrystalline thin film solar cells. In this context, the present work was performed on nanocrystalline Mo films deposited using RF magnetron sputtering under variable sputtering pressures and deposition temperatures. Interestingly, we found that the Mo films deposited at a relatively higher deposition temperature (≥200 °C) with a combination of optimum sputtering pressure exhibits high quality in terms of structural, mechanical, optical and electrical characteristics as desired for back-contact layer application in solar cells. Furthermore, efforts were made to understand the effect of microstructure on the phase stabilization, crystal structure, and electrical characteristics of Mo films as a function of deposition variables. We paid utmost attention to the structural and mechanical properties of thin Mo films (~105 ± 5 nm), compared to those reports on the relatively thicker Mo films in the literature, where the true effect of nanoscale dimensions is elucidated as a function of crystallite size, which is controlled by means of variable processing conditions. Our findings demonstrate that the processing conditions can be tuned to obtain Mo films with variable microstructures, which enables superior mechanical and electrical properties desired for CIS and CIGS solar cells. Based on the results, a size-structure-property correlation, which may be useful as a road-map to optimize the conditions to produce Mo-based materials for thin film solar cells, was established.

Table 1
Experimental conditions employed for Mo film deposition.

Parameter	Value
Base pressure	2×10^{-7} Torr
Sputtering power	100 W
Argon sputtering pressure	3-25 mTorr (T_s = 200 °C, constant)
Deposition temperature	25-500 °C (P_{Ar} = 5 mTorr, constant)
Target-to-substrate distance	7 cm
Substrate	Silicon (100)
Film thickness	~105 ± 5 nm

2. Experimental

2.1. Fabrication

Nanocrystalline Mo films were RF-sputter deposited onto chemically cleaned silicon (Si) (100) wafers. The deposition chamber was then evacuated to a base pressure of ~2×10^{-7} Torr. Mo target (Plasmaterials, Inc.) with a 2 inch diameter and 99.999% purity was employed for sputtering. To ensure lateral isotropy, the substrates were continuously rotated at a rate of 3–4 rpm during the deposition. The Ar flow was controlled using MKS mass flow meters. The deposition time was kept constant to obtain a film thickness of ~105 ± 5 nm. Before every deposition, the Mo target was pre-sputtered for at least 15–20 min while keeping the substrate shutter closed to facilitate stable plasma and to remove contaminants. The experimental conditions employed for the Mo film fabrication are listed in Table 1.

2.2. Characterization

The crystal structure analysis was performed using Grazing Incidence X-ray Diffraction (GIXRD) equipment (Bruker D8 advance, CuK_α radiation, and wavelength = 0.154 nm) at room temperature. The average crystallite size (d) was determined from the integral width of the diffraction lines, which is named as Scherrer's equation as follows: [43]

$$d = \frac{0.9\,\lambda}{\beta \cos\theta} \quad (1)$$

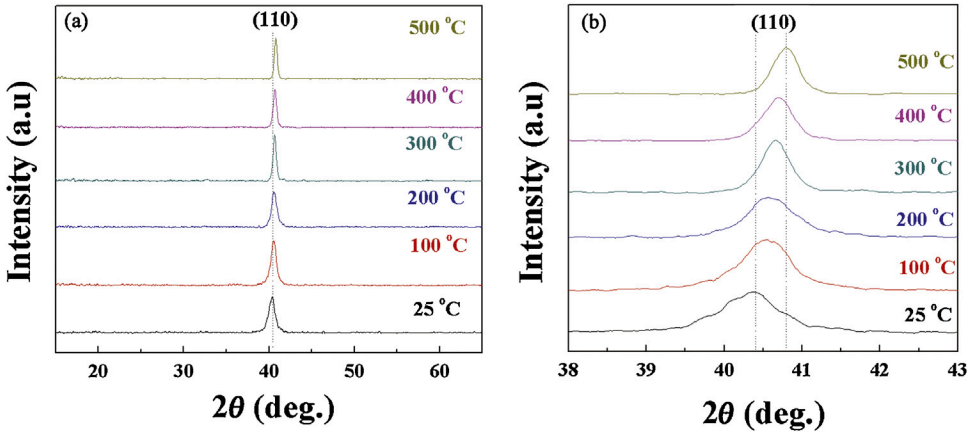

Fig. 1. (a) GIXRD patterns of Mo films deposited at various T_s and (b) high-resolution scans of the Mo (110). The peak observed at ~40.5° corresponds to diffraction from (110) crystal planes of body centered cubic (bcc) Mo. The (110) peak intensity increase with increasing T_s can be noted and the peak sharpens with a decrease in full width at half maxima (FWHM) with increasing T_s. In addition, a slight positive peak shift occurs with increasing T_s.

where λ is the wavelength of X rays, β is the width of the peak at its half intensity, and θ is the angle of the peak. The surface morphology analysis was performed using high performance and ultra-high-resolution scanning electron microscope (SEM, Hitachi S-4800). Optical properties of the Mo films were measured using CARY 5000 UV–vis–NR double-beam spectrophotometer in the range of 200–3000 nm. Ecopia HMS 3000 Hall measurement system was used to determine the electrical properties such as resistivity, carrier concentration and mobility. In this method, a current was applied to the test sample using four small contacts and the corresponding voltage was measured on a flat arbitrarily shaped sample of uniform thickness. The four electrode probes were placed at the periphery of the samples and on measurement, provided the average resistivity of the sample. Hall mobility and carrier concentration were also obtained during the measurement [44].

3. Results and discussion

3.1. Effect of deposition temperature

To understand the effects of deposition temperature on the structure, surface/interface morphology, and electrical properties, Mo films were deposited at varying temperature from 25 °C to 500 °C while keeping a constant deposition pressure of 5 mTorr. The results and analyses of all the characterization that were performed are presented and discussed below.

3.1.1. Crystal structure

The GIXRD patterns of Mo films deposited under variable T_s are presented in Fig. 1(a). The effect of temperature on the growth behavior is evident as reflected in the marked difference in XRD patterns of Mo films (Fig. 1(a)) as a function of T_s. The notable feature is the fact that all the Mo films exhibit the XRD peak at ~40.5° which corresponds to diffraction from (110) crystal planes of body centered cubic (bcc) Mo. This observation is an indication that the Mo films exhibit (110) preferential growth [15,45,46]. It can be also noted that the (110) peak intensity increases with increasing T_s from 25 to 500 °C. This behavior can be attributed to the improved crystalline quality with increasing T_s. The Mo films deposited at the highest T_s (500 °C) exhibit dominance in the (110) peak intensity (Fig. 1(a)). In order to better understand peak intensity variation and to drive quantitative information, high resolution scans were performed on the (110) reflection. The high-resolution scans of the (110) peak of Mo films are shown in Fig. 1(b). It is evident that the peak becomes sharp with a decrease in full width at half maximum (FWHM) along with a slight positive peak shift with increasing T_s. Considerable peak broadening noted for Mo films deposited at lower temperatures, (T_s = 25–100 °C) may be due to the presence of smaller crystallites. The average crystallite size increases from 9 to 22 (±1) nm with increasing T_s from 25 to 500 °C (presented in Fig. 2). From XRD data (Figs. 1 and 2), it is evident that the improved structural order along with an increase in the crystallite size accounts for the observed (110) peak sharpening and FWHM narrowing. Thus, XRD results confirm a clear dependence of crystallinity of Mo films on T_s. Interdependency between texture development and processing parameters in physical vapor deposited thin film can be, in general, explained based on thermodynamics or growth kinetics [15,45]. Therefore, the effects of T_s on the crystal structure and growth behavior of Mo films can be attributed to the differences in adatom mobility, which influences the texture and/or preferred orientation of the films grown.

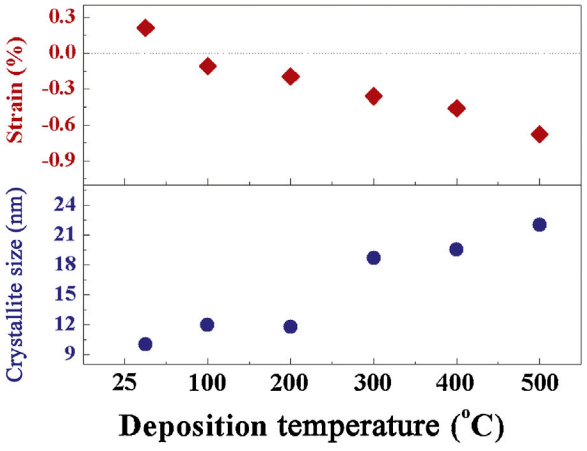

Fig. 2. Variation of average crystallite size and lattice strain of Mo films with T_s.

It is evident from the high-resolution scans that, as T_s increases, the (110) peak experiences a positive shift. The variation of the average lattice parameter i.e., the shift of the peak position, in the direction normal to the plane of the films gives the strain in Mo films. This lattice strain may be either tensile or compressive. The lattice strain for the films was determined using the relation [17]:

$$\text{Strain}\ (\%) = \frac{\Delta a}{a} \times 100 \qquad (2)$$

where a is the lattice parameter (for Mo reference, a = 0.31469 nm) [17,47]. In general, the strain of the films depends on voids, oxy-

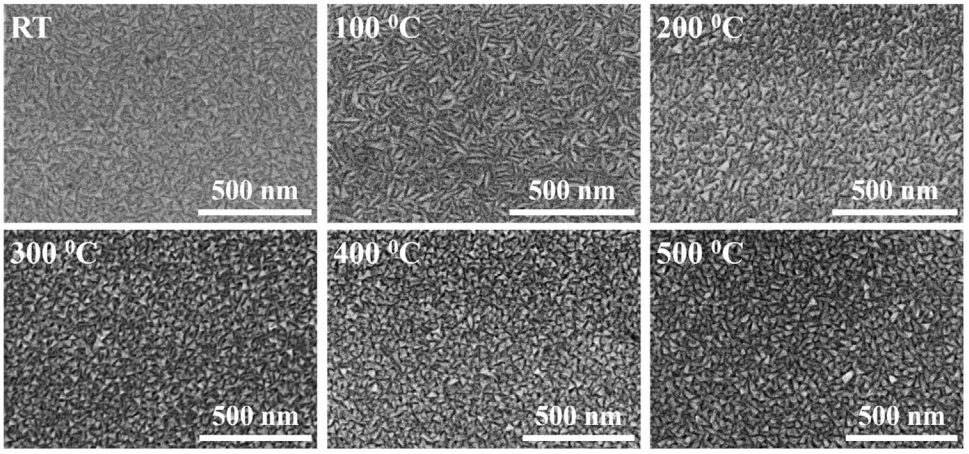

Fig. 3. Top-view SEM images of Mo films deposited under variable T_s.

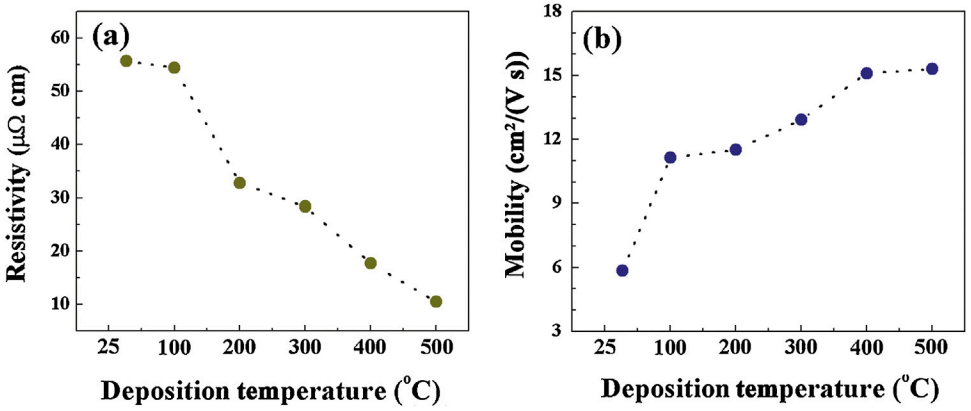

Fig. 4. Electrical characteristics of Mo films sputtered at different T_s: (a) electrical resistivity; (b) carrier mobility; (c) carrier concentration with T_s. It is evident that the electrical characteristics are strongly influenced by the deposition temperature.

gen or argon gas impurities, and crystallographic flaws [18]. Most of these Mo films were in compressive strain, as indicated by the results presented in Fig. 2. Note that the positive values represent the tensile nature while negative values are indicative of compressive nature. The surface roughness values for this set of Mo films were measured using atomic force microscopy (AFM) technique. The surface roughness is 1.24 nm for the Mo film deposited at 25 °C. By increasing the deposition temperatures the roughness values decrease to 0.51 nm for the film deposited at 400 °C. Increase in substrate temperature increases the thermal energy of the thin film, thereby facilitating higher adatom mobility, delivering smoother thin films at higher deposition temperatures.

3.1.2. Surface morphology

Fig. 3 shows the SEM images of Mo films deposited at various T_s. It can be seen that, not only the size, but also the grain shape is affected by T_s. All the Mo films exhibit granular morphology, which is characterized by the presence of grains with feather like shape and densely packed microstructure. The grains are noticeably visible, no evidence of voids is seen. The film deposited at 25 °C shows a flat and smooth surface with pebble like structure. At T_s = 100 °C, grains present sharp triangular tails. The films become smoother and the grains seem to break down into smaller ones for the films deposited at T_s = 200–400 °C. Mo films deposited at 500 °C exhibit the most compact morphology while there are no significant changes noted beyond 300 °C. The trend noted is that the grain elongation decreases with increasing T_s. In general, increasing the temperature will increase the adatom mobility in the thin films which results in greater diffusion leading to adjacent crystals merging together which directly facilitates surface morphology modification [35].

3.1.3. Electrical properties

In addition to structure and morphology, the electrical characteristics of Mo films are quite important for their integration into solar cells as back contact layers. The electrical characteristics of the Mo films deposited under variable T_s, namely carrier concentration, mobility, and resistivity, are shown in Fig. 4. The results indicate that the T_s and microstructure strongly influence the Mo electrical characteristics. The electrical resistivity variation as a function of T_s for nc-Mo films is shown in Fig. 4(a) with the films deposited at 25 °C exhibiting the highest resistivity (55 μΩ cm). It can be noted that the electrical resistivity of the Mo films decreases continuously with increasing T_s, with the lowest values corresponding to Mo films deposited at T_s = 300–500 °C, with the 500 °C sample in particular possessing electrical resistivity of 10 μΩ cm. This value is remarkably low not only within the set of these Mo films but also when compared to those reported in the literature [48]. Also, note that the electrical resistivity of the Mo films correlates with the average grain size variation and surface roughness. Increasing grain size and structural order tends to decrease the electrical resistivity [14,15]. This phenomenon is also coupled with the increase in the carrier mobility [12,15]. Increase in the average size increases the carrier mobility [12,40,49]. Therefore, the observed increase in the grain size of the Mo films with increasing T_s leads to a reduction in the grain boundary potential barrier's height and in the number of

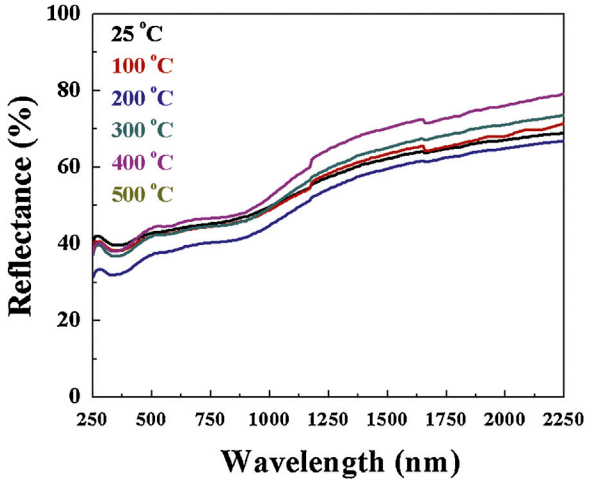

Fig. 5. Optical reflectance of Mo films deposited under variable T_s.

grain boundaries that the charge carrier has to cross during electrical transport [12]. This leads to decrease in the electrical resistivity of Mo films.

The variation in carrier mobility of Mo films as a function of T_s is represented in Fig. 4(b). The mobility is seen to increase continuously with increasing T_s. The mobility values in nc-Mo films increased from 5 to 15 $cm^2/(V\ s)$ for a variation in T_s from 25 to 500 °C, The hall mobility is increased due to the improvement in film crystallinity at higher temperatures, on the other hand which leads to decrease in resistivity [45,50].

The electrical carrier concentration variation as a function of T_s for nc-Mo films is shown in Fig. 4(c). The carrier concentration noted for Mo films deposited at T_s = 25 °C was 1×10^{22} cm^{-3}, which is lower among the set of Mo films deposited. However, the carrier concentration value increases with increasing T_s with the highest value of 1.01×10^{23} cm^{-3} noted for the Mo films deposited at 500 °C. This observed trend of carrier concentration corroborates with structure and morphology data and is mainly due to the crystallization and grain morphology [45,50].

3.1.4. Optical properties

Fig. 5 shows the reflectance of the Mo films deposited at various T_s. Reflectivity of the back contact layers is also one of crucial parameter to improve the overall efficiency of the solar cell. By maximizing the light reflectance of the back contact, more photons can be absorbed [12]. The SEM results indicate that the Mo films deposited at various temperatures shows elongated large stripe-shaped grain boundaries and large columnar grains over the film surface which influence the light scattering. The reflectance data of the nc-Mo films are in reasonable agreement with those reported in the literature [46]. The dense microstructure coupled with stress-free state of the Mo films with no porosity of the Mo films is ideal for solar cell applications.

3.2. Effect of sputtering pressure

To understand the effect of variable sputtering pressure on the structure, surface/interface morphology, electrical characteristics and optical properties, a set of Mo films were deposited by varying argon pressure from 3 mTorr to 25 mTorr while keeping the deposition temperature constant at 200 °C. The results and analyses of those Mo films are presented and discussed below.

3.2.1. Crystal structure

Similar to the GIXRD patterns of nc-Mo films deposited at various T_s, Mo films deposited under variable P_{Ar} also showed only one peak, at ~40.5°, which corresponds to diffraction from (110) planes. The detailed, high-resolution scan of the (110) peak is shown in Fig. 6(a). It is evident that the (110) peak intensity decreases and becomes broader with increasing P_{Ar} from 3 to 25 mTorr. Furthermore, the (110) peak position is observed to be shifting towards left as a function of P_{Ar}. This observation indicates a change in lattice parameter and, thus, stress state in the Mo films. It can be seen that there is a significant (110) peak intensity reduction coupled with peak broadening with increasing P_{Ar}. It appears that there is a degradation of the crystal quality with increasing P_{Ar} which may be due to the variation in the energy of the sputtered species. Generally, in a sputtering process, the energy of sputtered atoms and/or ions are influenced by the working pressure [22]. When P_{Ar} is higher, it enhances the probability of collisions between atoms, as such the energy of atoms will tend to decrease [12]. At low sputtering pressures, the frequency of the gas-phase bombardment will also decrease, due to an increase in the kinetic energy of the sputtered Mo atoms and neutral Ar atoms [1,14,18]. This enhances the atomic peening and tends to form a denser films [14,18]. Thus, with increasing P_{Ar}, the Mo atoms and gas ions collide more often which results in a decrease in the bombardment energy [12,18]. This reduced atomic mobility and peening produce less dense films [12]. For the films deposited at higher pressures, the peak shift and broadening are higher indicating the crystalline quality deterioration at higher P_{Ar}. The average crystallite size (d) was determined using Eq. (1). The maximum value of d is found to be 18 (±1) nm for P_{Ar} = 3 mTorr. With the increase in P_{Ar}, the size gradually decreases to 7 (±2) nm for a P_{Ar} of 19 mTorr. As generally noted in PVD films, the P_{Ar}-d relationship can be attributed to the reduction in the mean free path and associated surface damage. The detailed analysis about crystallite size and the effect of size on the mechanical properties of nc-Mo films deposited as a function of variable sputtering pressure has been reported elsewhere [51].

The lattice strain and FWHM of the Mo films deposited under variable P_{Ar} are presented in Fig. 6(b) and (c), respectively. The trend observed is a true effect of P_{Ar} on the structural quality of nc-Mo films. The origin of the lattice strain profiles in Mo films can be correlated with impurities, voids, and crystallographic flaws [17]. The Mo films exhibit a compressive strain for P_{Ar} = 3–9 mTorr, at which point there is a transformation to tensile nature. However, the strain values for most of the films are relatively close with a minimal variation (Fig. 6(b)) while the highest strain occurs in Mo films deposited at the highest P_{Ar} = 25 mTorr. As explained in the previous section, the changes in crystal structure and microstructure account for the strain variation as a function of processing parameters. The surface roughness values of Mo films deposited at various P_{Ar} lie between 2.05 nm to 0.70 nm. The nanocrystalline Mo films deposited at lower P_{Ar} exhibits higher surface roughness of 2.05 nm, which then progressively and continuously decreases to sub nm level i.e., 0.70 nm on increasing P_{Ar} to 25 nm. At low sputtering pressures, the frequency of the gas-phase bombardment will decrease, due to an increase in the kinetic energy of the sputtered Mo atoms which results in higher surface roughness.

3.2.2. Surface and interface morphology

The SEM images of the Mo films deposited under variable P_{Ar} are presented in Fig. 7. The films deposited at lower P_{Ar} exhibit a compact and smooth surface morphology. The thin film deposited at 3 mTorr presents pyramid shape structure with a corresponding crystal size of 18.0 (±1) nm (calculated form XRD). This phenomenon was observed upto the pressure of 5 mTorr. On further increasing the pressure to 14 mTorr, the pyramid shape texture transformed in to granular shape texture and the thin films

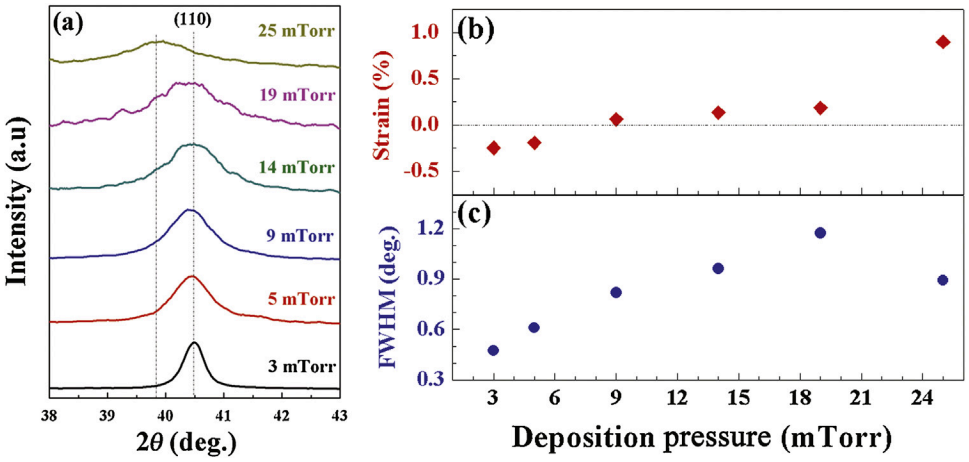

Fig. 6. GIXRD patterns of Mo films deposited at various P_{Ar}: (a) high resolution scan of Mo (110) peak; (b) lattice strain; (c) full width at half maximum of (110) peak.

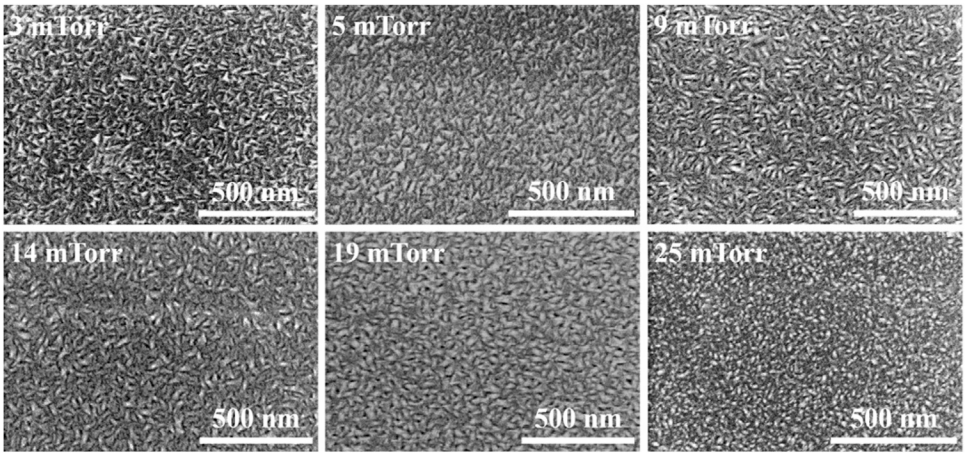

Fig. 7. SEM images of Mo films deposited under variable P_{Ar}.

deposited at 25 mTorr displays pyramid structure similar to that of 3 mTorr film [52]. However, increasing P_{Ar} seems to include voids on the surface resulting in a porous and loosely packed microstructure. The grains are densely packed with columnar structure when the Mo films were deposited at lower P_{Ar}. This morphology variation can be attributed to the variation in the kinetic energy of the sputtered species under variable P_{Ar} [2,14,18]. As the pressure increases, the grains evolve from irregular structures to triangular tapered structures. This phenomenon can be explained by the structure zone models [16]. The adatom mobility is controlled by adjusting the sputtering pressure. Usually, high sputtering pressures have ability to reduce adatom mobility and therefore can promote zone 1 structures with triangular tapered structure [16].

Fig. 8 shows the cross-sectional SEM images, which clearly indicate the characteristic interface morphology evolution of Mo films with P_{Ar}. The fractured samples or Mo films deposited on Si were mounted for sectional imaging to obtain the micrographs, where the Mo film and Si-substrate regions are indicated (Fig. 8). It is evident from these micrographs that the Mo films display the columnar structure at lower P_{Ar}. However, the morphology evolves into a dense packing structure at intermediate pressures and then finally to spattered morphology at very high P_{Ar} (19–25 mTorr). For samples deposited with variable deposition temperature keeping P_{Ar} at 5 mTorr, columnar interface microstructure was noted at all temperatures except at the highest T_s = 500 °C, where deterioration of properties is noted. Note that, as recognized widely in the literature, the sputter-deposited film interface microstructure is strongly

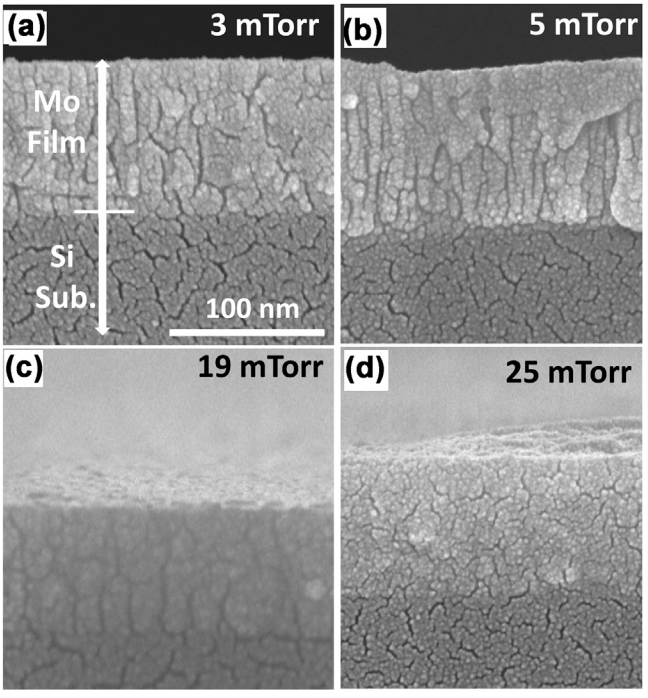

Fig. 8. Interface microstructure evolution in Mo films deposited under variable P_{Ar}.

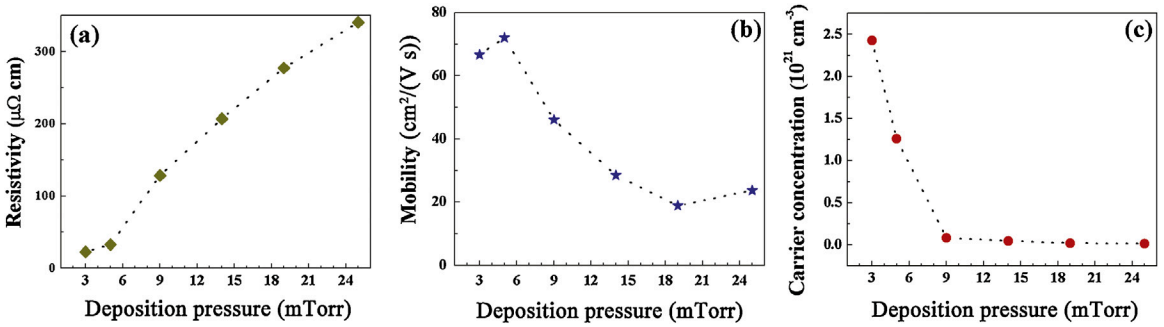

Fig. 9. Electrical characteristics of Mo films sputtered at different P_{Ar}: (a) electrical resistivity; (b) carrier mobility; (c) carrier concentration. It is evident that the electrical characteristics are strongly influenced by the deposition pressure.

dependent on the adatom or particle energy of the growing film. Thus, higher kinetic energy variations and diffusion of the impinging species may be the reason for observed microstructure changes in Mo films.

3.2.3. Electrical properties

Fig. 9 presents the electrical characteristics of Mo films deposited under variable P_{Ar}. The electrical resistivity, carrier concentration and mobility of Mo films deposited at various P_{Ar} are shown. The results indicate that the P_{Ar} has a strong influence on the electrical characteristics of Mo films. The resistivity of Mo films is found to be directly proportional to P_{Ar} (Fig. 9(a)) as at lower sputtering pressures i.e., 3 mTorr, the resistivity is low which then increases with increasing P_{Ar} and reaches 340 μΩ cm for the Mo film deposited at P_{Ar} = 25 mTorr. This resistivity variation can be attributed to the fact that, at higher P_{Ar}, the kinetic energy of Mo ions is reduced due to the increased particle scattering [3,14]. As a result of that, degradation of the film crystallinity and grain growth occurs leading to less dense and porous column boundaries which implies a higher electrical resistivity [1,14]. On the other hand, at lower P_{Ar}, incident atoms contain lighter energy because of lesser scattering which tends to impart higher momentum to Mo atoms to form more crystalline films with densely packed structures. As a result, better crystallinity and smooth grain growth tends to lower electrical resistivity of the Mo films.

The variation in carrier mobility of Mo films as a function of P_{Ar} is represented in Fig. 9(b). The mobility decreases continuously with increasing sputtering pressure since there is a decrease in the energy of the discharged atoms [3]. The species arriving on substrate surface has lower mobility, and the films exhibit porous columnar grain with intergranular voids (discussed in SEM). The electron mobility variation is corroborated with the structure and morphology variation with P_{Ar}. When the P_{Ar} is increased from 3 to 25 mTorr, the mobility value decreases from 67 to 23 $cm^2/(V\,s)$. One of the primary reason for decrease in mobility is due to the increase in grain boundaries.

The variation in carrier concentration as a function of P_{Ar} is shown in Fig. 9(c). The carrier concentration has a noted maximum (2.42×10^{22} cm^{-3}) in the Mo film deposited at P_{Ar} = 3 mTorr. The carrier concentration decreases with increasing P_{Ar}; it reaches the lowest value of 8.37×10^{20} cm^{-3} for the Mo film deposited at P_{Ar} = 9 mTorr and then continues to be low for all the depositions made in the P_{Ar} range of 9–25 mTorr.

3.2.4. Optical properties

The measured optical reflectance of Mo films deposited at variable sputtering pressure is shown in Fig. 10. As observed in the figure, the reflectance gradually decreases with increasing P_{Ar} and 5 mTorr film demonstrates the highest reflectance. This trend is also apparent with wavelength [3,12]. This variation is noted mainly in

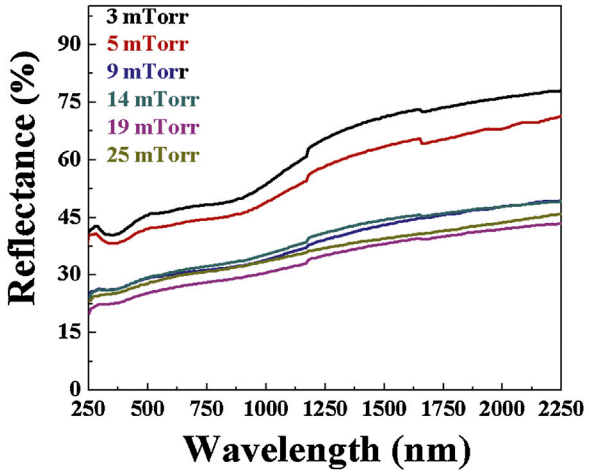

Fig. 10. Optical reflectance of Mo films as a function of P_{Ar}.

two cases. The very first characteristic is surface roughness. Yoon et al. reported that, the surface roughness is linearly proportional with the working pressure [12]. The surface roughness can reduce the amount of reflected light. Porosity is also one of the characteristics which can influence the reflectance [2]. As discussed, surface roughness is decreased by increasing the deposition pressure. The surface light scattering due to roughness can affect the amount of reflected light perpendicular to the surface. Therefore, the variation of the reflectance of the incident light from Mo surface is due to surface scattering effects. Apart to the scattering, the Mo films deposited at higher pressure possess a loosely packed porous structures as discussed in previous sections an act as another reason for the reduction in the reflectance spectra.

Finally, we would like to highlight the importance of the present work in the context of utilizing such Mo films for electronic device applications by considering the example or case of solar cells. The solar cell is a multilayer component device, which converts sunlight into electricity on the basis of internal photo-effect [1,12–19]. The back contact is the final layer and is very important for CIS or CIGS solar cells. The most important and critical issue in the CIS or CIGS or CdTe/CdS solar cell production is to form a low-resistive and stable ohmic contact with the respective p-type photo-absorber materials. Magnetron sputter-deposited Mo thin films are widely used as back electrodes in thin-film solar cells. It can be noted that the values reported in the present work vary in the range of 10–350 μΩ cm depending on the sputtering pressure and substrate temperature employed for Mo film deposition. Note that the Mo films not only exclusively serve the purpose of an electrical back contact but also act as a kinetic diffusion barrier for the constituting elements of the neighboring component layers. Since the stability at process-

ing temperatures (up to 600 °C) coupled with chemical inertness of Mo is well known, the chemical composition and structural stability of the Mo films in the T_s range of employed in this work is not at all a concern. However, we believe that the improved structural quality and morphology are the primary reason for the observed low resistivity values for the Mo films deposited at elevated temperatures. The electrical resistivity was found to be more sensitive to the working pressure. The low electrical resistivity was obtained only at lower P_{Ar} (3–6 mTorr). The resistivity increase at higher P_{Ar} is not suitable for solar cell device applications. Therefore, we conclude that the Mo films with low resistivity can be obtained in the T_s range of 200–500 °C while keeping the most critical parameter of working pressure at P_{Ar} = 3–5 mTorr. Furthermore, sputtering techniques are widely used in industrial processes, especially, the multilayered solar cell devices' fabrication, because high quality films can be obtained by carefully controlling the processing conditions. Sputter-deposition of materials and multilayered devices offer the key significant advantages of: (1) ease of sputtering of any metal, alloy or compound, (2) high-purity films, (3) excellent adhesion, and (4) excellent coverage uniformity on large-area substrates. Therefore, scaling up the process to produce Mo films in real/practical applications is also possible.

4. Conclusion

Molybdenum thin films were deposited at different sputtering pressure and deposition temperature values, which were varied in the range of 3–25 mTorr and 25-500 °C, respectively. The crystal structure, surface morphology, stress state, electrical characteristics and optical properties of Mo films were evaluated as a function of P_{Ar} and T_s. Such a detailed study enabled the optimization of experimental conditions to realize superior quality Mo films for application in thin film solar cells. The XRD and SEM analyses indicate that the effects of T_s and P_{Ar} are significant on the crystal structure, morphology and texturing of the nc-Mo films. The average crystallite size increases from 9 to 22 (±1) with increasing T_s from 25 to 500 °C. The electrical resistivity of Mo film decreases from 55 μΩ cm to 10 μΩ cm for T_s = 25–500 °C; however, the low resistive Mo films were obtained only in the 200–500 °C range. The effect of sputtering pressure is critically important in optimizing the microstructure, which in turn influences the electrical and optical characteristics of Mo films. At low P_{Ar} (3–6 mTorr), Mo films were densely packed with good structural properties, whereas Mo films became porous and loosely packed microstructures with increasing P_{Ar}. The low resistive (10–20 μΩ cm) Mo films, which can be realized by selectively depositing films at lower P_{Ar}, with reasonably good structural and optical properties are suitable for solar cell device applications while the processing temperature can be selectively tuned in the range of 200–500 °C depending on the specific design.

Acknowledgement

This work was supported financially by the National Science Foundation (NSF) with the NSF-PREM grant #DMR-1827745.

References

[1] N. Dhar, P. Chelvanathan, M. Zaman, K. Sopian, N. Amin, Energy Proc. 33 (2013) 186–197.
[2] N. Akcay, N.A. Sonmez, E. Zaretskaya, S. Ozcelik, Curr. Appl. Phys. 18 (2018) 491–499.
[3] M. Jubault, L. Ribeaucourt, E. Chassaing, G. Renou, D. Lincot, F. Donsanti, Sol. Energy Mater. Sol. Cells 95 (2011) S26–S31.
[4] S. De Wolf, A. Descoeudres, Z.C. Holman, C. Ballif, Green 2 (2012) 7–24.
[5] Z.H. Li, E.S. Cho, S.J. Kwon, Appl. Surf. Sci. 257 (2011) 9682–9688.
[6] X. Xu, S. Li, J. Chen, S. Cai, Z. Long, X. Fang,Adv. Funct. Mater. 28 (2018), 18020291.
[7] X. Fang, L. Zhang, J. Mater. Sci. Technol. 22 (2006) 1–18.
[8] M.R. Leyden, L. Meng, Y. Jiang, L.K. Ono, L. Qiu, E.J. Juarez-Perez, C. Qin, C. Adachi, Y. Qi, J. Phys. Chem. Lett. 8 (2017) 3193–3198.
[9] W. Yang, K. Hu, F. Teng, J. Weng, Y. Zhang, X. Fang, Nano Lett. 18 (2018) 4697–4703.
[10] D. Li, X. Shu, D. Kong, H. Zhou, Y. Chen, J. Mater. Sci. Technol. 34 (2018) 2027–2034.
[11] X. Mathew, J.P. Enriquez, A. Romeo, A.N. Tiwari, Sol. Energy 77 (2004) 831–838.
[12] J.H. Yoon, S. Cho, W.M. Kim, J.K. Park, Y.J. Baik, T.S. Lee, T.Y. Seong, J.H. Jeong, Sol. Energy Mater. Sol. Cells 95 (2011) 2959–2964.
[13] P.C. Huang, C.H. Huang, M.Y. Lin, C.Y. Chou, C.Y. Hsu, C.G. Kuo, Int. J. Photoenergy 2013 (2013) 1–8.
[14] Z.H. Li, E.S. Cho, S.J. Kwon, Appl. Surf. Sci. 257 (2011) 9682–9688.
[15] J.H. Cha, K. Ashok, N.J.S. Kissinger, Y.H. Ra, J.K. Sim, J.S. Kim, C.R. Lee, J. Korean Phys. Soc. 59 (2011) 2280–2285.
[16] X. Dai, A. Zhou, L. Feng, Y. Wang, J. Xu, J. Li, Thin Solid Films 567 (2014) 64–71.
[17] H. Khatri, S. Marsillac,J. Phys. Condens. Matter 20 (2008), 055206.
[18] G. Zoppi, N.S. Beattie, J.D. Major, R.W. Miles, I. Forbes, J. Mater. Sci. 46 (2011) 4913–4921.
[19] J. van Deelen, C. Frijters, Sol. Energy 143 (2017) 93–99.
[20] P. Sinsermsuksakul, K. Hartman, S.B. Kim, J. Heo, L. Sun, H.H. Park, R. Chakraborty, T. Buonassisi, R.G. Gordon,Appl. Phys. Lett. 102 (2013), 053901.
[21] J.H. Scofield, A. Duda, D. Albin, B. Ballard, P. Predecki, Thin Solid Films 260 (1995) 26–31.
[22] D.W. Hoffman, J.A. Thornton, J. Vac. Sci. Technol. 20 (1982) 355–358.
[23] J.J. Scragg, J.T. Watjen, M. Edoff, T. Ericson, T. Kubart, C. Platzer-Björkman, J. Am. Chem. Soc. 134 (2012) 19330–19333.
[24] K. Orgassa, H.W. Schock, J. Werner, Thin Solid Films 431 (2003) 387–391.
[25] J. Bartolome, M. Diaz, J. Requena, J. Moya, A. Tomsia, Acta Mater. 47 (1999) 3891–3899.
[26] T. Wada, N. Kohara, S. Nishiwaki, T. Negami, Thin Solid Films 387 (2001) 118–122.
[27] R. Tran, Z. Xu, N. Zhou, B. Radhakrishnan, J. Luo, S.P. Ong, Acta Mater. 117 (2016) 91–99.
[28] G. Martinez, C.V. Ramana, AIP Adv. 7 (2017) 1–8.
[29] K.S. Harsha, Principles of Vapor Deposition of Thin Films, Elsevier, 2015.
[30] P.G. Dubey, J. Manandhar, S. Shutthanandan, V. Ramana, Sol. Energy 166 (2018) 146–158.
[31] B.S. Yadav, A.C. Badgujar, S.R. Dhage, Sol. Energy 157 (2017) 507–513.
[32] K.H. Ong, R. Agileswari, B. Maniscalco, P. Arnou, C.C. Kumar, J.W. Bowers, M.B. Marsadek, Int. J. Photoenergy 33 (2018) 723–729.
[33] K.A. Kress, G.J. Lapeyre, J. Opt. Soc. Am. 60 (1970) 1681–1684.
[34] D. Guo, Z. Wu, Y. An, X. Li, X. Guo, X. Chu, C. Sun, M. Lei, L. Li, L. Cao, J. Mater. Chem. C 3 (2015) 1830–1834.
[35] X. Jia, Z. Lin, T. Yang, B. Puthen-Veettil, L. Wu, G. Conibeer, I. Perez-Wurfl, Appl. Sci. 8 (2018) 1692.
[36] P. Bommersbach, L. Arzel, M. Tomassini, E. Gautron, C. Leyder, M. Urien, D. Dupuy, N. Barreau, Prog. Photovolt. 21 (2013) 332–343.
[37] M. Theelen, F. Daume, Sol. Energy 133 (2016) 586–627.
[38] D. Fernández-González, Í. Ruiz-Bustinza, C. González-Gasca, J.P. Noval, J. Mochón-Castaños, J. Sancho-Gorostiaga, L.F. Verdeja, Sol. Energy 170 (2018) 520–540.
[39] J. Waldron, D. Juenker, J. Opt. Soc. Am. 54 (1964) 204–207.
[40] J.H. Yoon, S. Cho, W.M. Kim, J.K. Park, Y.J. Baik, T.S. Lee, T.Y. Seong, J.H. Jeong, Sol. Energy Mater. Sol. Cells 95 (2011) 2959–2964.
[41] S. Wang, C. Hsu, F. Shiou, P. Huang, D. Wen, J. Korean Inst. Electr. Electron. Mater. Eng. 42 (2013) 71–77.
[42] R. Zhang, Z. Huo, X. Jiao, B. Du, H. Zhong, Y. Shi, J. Nanosci. Nanotechnol. 16 (2016) 8154–8159.
[43] B. Cullity, Elements of X-ray Diffraction, Addison-Wesley Publishing Co., Inc., USA, 1956, p. 78.
[44] S. Thirumavalavan, Y. Mani, S.S. Suresh, J. Nano-Electron. Phys. 7 (2015) 040241–040244.
[45] H. Ahn, D. Lee, Y. Um, Appl. Sci. Converg. Technol. 26 (2017) 11–15.
[46] J.H. Yoon, K.H. Yoon, W.M. Kim, J.K. Park, Y.J. Baik, T.Y. Seong, J.H. Jeong,J. Phys. D 44 (2011), 4253021.
[47] W. Li, X. Yan, A.G. Aberle, S. Venkataraj,J. Appl. Phys. 54 (2015), 08KC141.
[48] S. Siol, T.P. Dhakal, G.S. Gudavalli, P.P. Rajbhandari, C. DeHart, L.L. Baranowski, A. Zakutayev, ACS Appl. Mater. Interf. 8 (2016) 14004–14011.
[49] L. Krusin-Elbaum, M. Aboelfotoh, T. Lin, K. Ahn, Thin Solid Films 153 (1987) 349–358.
[50] Y.C. Lin, W. Yen, L. Wang, Chin. J. Phys. 50 (2012) 82–88.
[51] A.K. Battu, V.B. Zade, E. Deemer, C.V. Ramana,Adv. Eng. Mater. 20 (2018), 18004961.
[52] D. Zhou, H. Zhu, X. Liang, C. Zhang, Z. Li, Y. Xu, J. Chen, L. Zhang, Y. Mai, Appl. Surf. Sci. 362 (2016) 202–209.